Journal of
Materials Chemistry A

ARTICLE

On the mechanism of photocatalytic reactions on $Cu_xO@TiO_2$ core-shell photocatalyst

Received 00th January 20xx,
Accepted 00th January 20xx

DOI: 10.1039/x0xx00000x

Kunlei Wang,[ab] Zuzanna Bielan,[ac] Maya Endo-Kimura,[a] Marcin Janczarek,*[d] Dong Zhang,[ae] Damian Kowalski,[f] Anna Zielińska-Jurek,[c] Agata Markowska-Szczupak,[g] Bunsho Ohtani[ae] and Ewa Kowalska*[ae]

Titania (titanium(IV) oxide) is highly active, stable, cheap and abundant photocatalyst, and thus commonly applied in various environmental applications. However, two main shortcomings of titania, i.e., charge carriers' recombination and inactivity under visible-light (vis) irradiation should be overcome for broad commercialization. Accordingly, titania has been doped, surface modified and coupled with various ions/compounds, including narrower bandgap semiconductors, such as oxides of copper and silver. Unfortunately, these oxides are not as stable as titania, and thus loss of activity under long-term irradiation (photo-corrosion) has been observed. Therefore, this study has focused on the preparation of stable coupled photocatalysts, i.e., $Cu_xO@TiO_2$ core-shell nanostructure by microemulsion method from commercial Cu_2O as a core and TiO_2 (ST01-fine anatase) as a shell. Photocatalysts have been characterized by DRS, SEM, TEM, XRD, XPS and reversed double-beam photo-acoustic spectroscopy (RDB-PAS) methods, and activity tests under UV (anaerobic dehydrogenation of methanol and oxidative decomposition of acetic acid) and vis (phenol oxidation) irradiation. The higher activities of coupled photocatalysts than their counterparts have been found in all studied systems under UV/vis irradiation. Moreover, long-term experiments (10 h) have shown high stability of Cu_xO/TiO_2. However, the change of oxidation state of copper has also been observed, i.e., to the negative and positive values, confirming the charge transfer according to Z-scheme under UV irradiation and type-II heterojunction under vis irradiation, respectively. The property-governed activity and the mechanism clarification have been discussed in detail.

1. Introduction

The development of photocatalytic processes is still mainly connected with materials based on titanium(IV) oxide (TiO_2, titania), which has been widely known as an efficient, stable and green semiconductor with photocatalytic performance used in water treatment, air purification, synthesis of chemical compounds, self-cleaning surfaces and renewable energy processes, such as photocurrent generation and water splitting for hydrogen production.[1-6] Although titania has been recognized as one of the best photocatalysts, two main shortcomings must be overcome for broader and commercial application, i.e., charge carriers' recombination (typical for all semiconductors), and inactivity under vis irradiation (due to wide-bandgap of titania, i.e., ca. 3.0-3.2 eV).

To overcome these limitations, different strategies in the preparation of titania-based materials have been considered, e.g., (i) doping with cations and anions, (ii) surface modification with various molecules and particles, (iii) formation of advanced-morphology materials (faceted, mesocrystals, inverse opals), and (iv) coupling with other semiconductors.[7] Accordingly, the design of coupled photocatalysts, composed of TiO_2 and other metal oxides, to establish the heterojunction is an important way to enhance the charge carrier (electron-hole) separation (increasing the lifetime of charge carriers) and to obtain vis-responsive materials (in the case of oxides with narrower bandgap than that of titania).[8] Copper oxides (p-type semiconductors) have been considered as good candidates to form the efficient heterojunction with TiO_2, i.e., Cu_2O and CuO with bandgap energies of ca. 2.1 eV and 1.7 eV, respectively. In particular, among copper oxides, the selection of Cu_2O opens the promising strategy to prepare the hybrid photocatalysts with high activity and good antipathogenic properties.[9, 10] Moreover, the Cu_2O/TiO_2 p-n heterojunction has been

[a] Institute for Catalysis (ICAT), Hokkaido University, N21 W10, 001-0021 Sapporo, Japan. E-mail: kowalska@cat.hokudai.ac.jp
[b] Northwest Research Institute, Co. Ltd. of C.R.E.C., 730000, Lanzhou, P.R. China
[c] Department of Chemical Technology, Faculty of Chemistry, Gdansk University of Technology (GUT), G. Narutowicza 11/12, 80-233 Gdansk, Poland
[d] Institute of Chemical Technology and Engineering, Faculty of Chemical Technology, Poznan University of Technology, 60-965 Poznan, Poland. E-mail: marcin.janczarek@put.poznan.pl
[e] Graduate School of Environmental Science, Hokkaido University, 060-0810 Sapporo, Japan
[f] Faculty of Chemistry and Biological and Chemical Research Centre, University of Warsaw, Zwirki i Wigury 101, 02-089 Warsaw, Poland
[g] Department of Chemical and Process Engineering, West Pomeranian University of Technology in Szczecin, Al. Piastow 42, 71-065 Szczecin, Poland
† Footnotes relating to the title and/or authors should appear here.
Electronic Supplementary Information (ESI) available: [details of any supplementary information available should be included here]. See DOI: 10.1039/x0xx00000x

described as an efficient photocatalyst for degradation of organic compounds and hydrogen generation.[8, 11-14] It has been reported that even simple physical mixing of copper(I) oxide and titania (grinding) results in the formation of efficient photocatalyst.[13] The high efficiency of such material has been observed for UV/Vis-induced acetic acid oxidation, and two mechanistic variants of this heterojunction depending on the form of TiO_2 have been suggested: Z-scheme and heterojunction-type II for anatase and rutile-based samples, respectively. Furthermore, Cu_2O/TiO_2 photocatalysts have exhibited high bactericidal and fungicidal properties.[13] However, the loss in the activity during long-term irradiation has been observed because of the low stability of Cu_2O (photocorrosion), i.e., dissolution of copper from the photocatalyst surface (e.g., $Cu^+ \rightarrow Cu^{2+}$).[15, 16] Therefore, the hindering of copper loss during photocatalytic reactions is the most important goal for efficient and stable Cu_2O/TiO_2 photocatalysts. For example, Wang et al. has proposed that titania protective layer on Cu_2O has significantly increased the stability and activity of Cu_2O/CuO photocatalyst.[17]

The design of the coupled photocatalysts is also connected with the character of interactions between two main components (metal oxides) forming the heterojunction. It has been proposed that the formation of core–shell structures is the promising strategy since such materials show the integration of individual components into a functional system that brings an improvement of physical and chemical properties (e.g., stability, dispersibility, multi-functionality), which could not be achieved for the components without good and/or stable contact.[18, 19] Particularly, the core@shell TiO_2-structured materials have been reported as recommended not only due to enhanced activity and stability, but also improved separability, e.g., when magnetic oxides are used as a core.[20, 21] Considering Cu_2O, the main problem comes from its poor stability (photocorrosion) in an aqueous environment. Therefore, the preparation of Cu_2O(core)@TiO_2(shell) systems might allow to avoid this phenomenon, and consequently improve the overall photocatalytic performance. Su at al. have obtained stable core–shell Cu_2O/TiO_2 nanocomposites, in which TiO_2 layer has uniformly covered each Cu_2O octahedral particle.[22] In other works, Cu_2O photocathode, protected by a thin coating of Al-doped ZnO/TiO_2 or TiO_2 layer, exhibits high activity for photoelectrochemical water reduction, photoelectrocatalysis and CO_2 reduction.[23-25] In the present study, the microemulsion method, successfully applied to synthesize the core–shell structured titania-based materials (e.g., magnetic photocatalysts)[26], has been applied for the first time to prepare the core–shell $Cu_xO@TiO_2$ photocatalysts.

2. Materials and methods

Two commercially available TiO_2 photocatalysts: P25 (AEROXIDE® TiO_2 P25, mixed-phase titania, specific surface area (SSA) = 52 m^2/g and crystal sizes equal to ca. 25 nm and 40 nm for anatase and rutile, respectively,[27] Nippon Aerosil, Tokyo, Japan) and ST01 (ST-01, fine anatase, SSA = 298 m^2/g and crystal size of 8 nm, Ishihara Sangyo, Osaka, Japan) have been used in this study, i.e., P25 as a reference titania sample (known as one of the most active titania photocatalysts) and ST01 as a shell layer. Cuprous oxide, used as a core, was supplied by Wako Pure Chemicals, Tokyo, Japan. Other chemicals, including cyclohexane, isopropanol, acetone, hydrochloric acid, ammonia solution, methanol, acetic acid, cetyltrimethylammonium bromide (CTAB, 98%) and dioctyl sulfosuccinate sodium salt (AOT) were provided by Wako Pure Chemicals. All reagents were used of analytical grade, and thus without further purification.

Preparation of $Cu_2O@TiO_2$ core-shell heterojunction

The water-in-oil (w/o) microemulsion method was applied for the preparation of $Cu_xO@TiO_2$ core-shell photocatalysts. In this system, the nanodroplets of aqueous phase have been dispersed in continuous oil phase, stabilized by the surfactant and co-surfactant at the w/o interface. The Cu_2O core was successfully covered with the titania shell layer using the changes in Zeta potential of Cu_2O and TiO_2 as a function of pH value (Fig. 1), firstly proposed by Zielińska-Jurek et al. for $Fe_3O_4@SiO_2@TiO_2$ (core/interlayer/shell) particles.[26] The $Cu_xO@TiO_2$ photocatalysts were obtained by two variants, i.e., in acidic (pH < 5) and basic (pH > 11) conditions. In acidic variant, cuprous oxide was dispersed in anionic AOT water solution and the pH was set to the value of 5 by adding of 0.1 M HCl solution. Molar ratio between water and surfactant was set at 30. The prepared solution was then dropwise added to cyclohexane/isopropanol (100:6 volume ratio) oil phase and stirred for 2 h to stabilize microemulsion. After stabilization, corresponding amount of TiO_2 was added to the system and stirred for 18 h. Afterwards, microemulsion was destabilized with acetone, washed with deionized water, dried at 80 °C for 24 h and ground in an agate mortar. Similar procedure was performed in basic variant, but with cationic CTAB as surfactant and at pH value of 11, set by ammonia solution. The junction between Cu_2O core and TiO_2 shell was promoted by their opposite surface charges, provided by the presence of anionic and cationic surfactants at acidic and basic conditions, respectively. The Cu_2O content was set to 1, 2, 5, 10 and 50 weight % of titania.

The radius of the water in oil droplets (R_w) has been calculated, based on the equation 1 (eq. 1),[28] reaching ca. 2.3 µm. Therefore, it has been assumed that the efficient coverage of Cu_2O core with TiO_2 shell inside the micelle is possible considering the sizes of their crystallites, i.e., ca. 88 nm for Cu_2O and 8 nm for TiO_2 (and even aggregated particles, i.e., 100-1000 nm and 20-60 nm, respectively, as shown in Fig. SX in ESI).

$$R_w = \frac{3V_{aq}}{\sigma} \cdot \frac{[H_2O]}{[S]} \quad [nm] \qquad (1)$$

where:

V_{aq} – volume of water molecules (water volume) [dm^3], σ – the area per polar head [nm^2], $[H_2O]/[S]$ – water/surfactant ratio; For CTAB the σ value is $4.23 \cdot 10^{-4}$ nm^2, according to Haq et al., [29]

and V_{aq} and $[H_2O]/[S]$ have been set to 0.0108 dm^3 and 30, respectively, resulting in R_w of $2.29 \cdot 10^3$ nm.

Characterization of photocatalysts

The morphology of samples and distribution of elements were investigated by scanning transmission electron microscopy, equipped with an energy-dispersive X-ray spectroscopy (STEM-EDS, HD-2000, HITACHI, Tokyo, Japan). Specific surface area of samples was estimated by nitrogen adsorption at 77 K using the Brunauer–Emmett–Teller (BET) equation. Photoabsorption properties of prepared photocatalysts were analyzed by diffuse reflectance spectroscopy (DRS; JASCO V-670 equipped with a PIN-757 integrating sphere, JASCO, LTD., Pfungstadt, Germany). Barium sulfate and bare titania (ST01) were used as reference for DRS analysis. Crystalline properties were analyzed by X-ray powder diffraction (XRD; Rigaku intelligent XRD SmartLab with a Cu target, Rigaku, LTD., Tokyo, Japan). Crystallite sizes of anatase, rutile and copper were estimated using the Scherrer equation. The chemical composition of the surface (content and chemical state of elements, i.e., titanium, oxygen and copper) was determined by X-ray photoelectron spectroscopy (XPS; JEOL JPC-9010MC with MgKα X-ray, JEOL, LTD., Tokyo, Japan). The dependence of the surface charge of bare semiconductors on the pH value was measured as Zeta potential. 0.1 g of semiconductor (Cu_2O or TiO_2) was dispersed in 100 ml of distilled water and continuously stirred using magnetic stirrer. The pH value was set by 0.1 M HCl and 0.1 M NaOH solutions, and the changes were monitored using Elmetron Multifunction meter CX-505 with EPS-1 14600/14 pH electrode (Elmetron, Zabrze, Poland). After pH-value was set, the sample was taken with a syringe and placed in a disposable folded capillary cell DTS1070 (Malvern Instruments Ltd., Malvern, UK). The measurement of Zeta potential was taken using Malvern Nano Zetasizer (Malvern Instruments Ltd., Malvern, UK).

The energy-resolved distribution of electron traps (ERDT) patterns and conduction band bottom (CBB) position were analyzed by reversed double-beam photoacoustic spectroscopy (RDB-PAS) and photoacoustic spectroscopy (PAS), respectively, as described elsewhere.[30] In brief, for RDB-PAS measurement, the sample was filled in a stainless-steel sample holder in a home-made PAS cell, equipped with an electret condenser microphone and a Pyrex window in the upper side. Methanol-saturated nitrogen was flowed through the cell for 30 min, the cell was irradiated by a 625-nm light-emitting diode beam (Luxeon LXHL-ND98, LUMILEDS, San Jose, CA, USA), modulated at 35 Hz by a function generator (DF1906, NF Corporation, Yokohama, Japan) as modulated light, and a monochromatic light beam from a Xe lamp (ASB-XE-175, Spectral Products, Putnam, CT, USA), equipped with a grating monochromator (CM110 1/8 m, Spectral Products, CT, USA) as continuous light. The continuous light was scanned from 650 to 300 nm with a 5-nm step. The RDB-PA signal was detected by a digital lock-in amplifier (LI5630, NF Corporation). Obtained spectrum was differentiated from the lower-energy side and calibrated with the reported total electron-trap density in units of μmol g^{-1}, measured by a photochemical method[31] to obtain an ERDT pattern. For PAS measurements, the cell window was irradiated from 650 to 300 nm by a light beam from a Xe lamp (ASB-XE-175, Spectral Products) with a grating monochromator (CM110 1/8m, Spectral Products, CT, USA) modulated at 80 Hz by a light chopper (5584A, NF Corporation, Japan) to detect the PAS signal using a digital lock-in amplifier, and then photoacoustic (PA) spectra were calibrated with a reference of PA spectrum of graphite. The CBB, as energy from the top of the valence band (VBT), of samples was calculated from the onset wavelength corresponding to the bandgap of samples.

Photocatalytic activity tests

The photocatalytic activity of samples was evaluated under UV/vis irradiation for: (1) oxidative decomposition of acetic acid (CO_2 system; CO_2 evolution), and (2) anaerobic dehydrogenation of methanol (H_2 system; H_2 evolution), and under vis irradiation for (3) oxidation of phenol. For activity tests, (1-2) 50 mg and (3) 10 mg of photocatalyst was suspended in 5 mL of aqueous solution of (1) acetic acid (5 vol%), (2) methanol (50 vol%), and (3) 0.21 mmol/L phenol in 35-mL Pyrex test tubes. The tubes were sealed with rubber septa, the suspensions were continuously stirred in a thermostated water bath and irradiated by (1-2) Hg lamp ($\lambda > 220$ nm) and (3) Xe lamp ($\lambda > 420$ nm; water IR filter, cold mirror and cut-off filter Y-45, in a reactor shown in Ref.[32]). For methanol dehydrogenation, suspensions containing titania and methanol were 15-min pre-bubbled with Ar to remove oxygen from the system. The amounts of (1) generated hydrogen, (2) liberated carbon dioxide, (3) phenol and benzoquinone (main degradation product) were determined by chromatography: (1-2) GC-TCD (detection of gas phase amount for every (1) 20 min and (2) 15 min, and (3) HPLC.

Commercial titania P25 (Degussa/Evonik) was used as a reference sample since P25 has exhibited one of the highest photocatalytic activity among various titania samples in different reaction systems (oxidation and reduction[27, 33, 34]), and thus is commonly used as a "standard" titania sample.

3. Results and discussion

Preparation of $Cu_2O@TiO_2$ core-shell particles

The zeta potential values as a pH-value function of the suspensions of bare Cu_2O and TiO_2 samples are shown in Fig. 1. The analysis is crucial for the proper selection of the microemulsion environment, particularly pH value and surfactant kind, in order to develop the efficient coverage of Cu_2O with TiO_2. It is known that titania nanoparticles (NPs) are positively charged at pH value below 5. Indeed, in the case of ST01 titania suspension, the isoelectric point (IEP; Zeta potential equal to zero) appears at the pH value of ca. 6.3. The IEP of cuprous oxide occurs almost in the whole range of pH value between 8 and 9. Above and below these values NPs are negatively and positively charged, respectively.

In the present study, $Cu_xO@TiO_2$ photocatalysts have been obtained by two variants of microemulsion method, i.e., in acidic ($pH < 5$) and basic ($pH > 11$) conditions. For the successful

covering of Cu_2O by the TiO_2 shell, it is necessary to introduce charge-changing surfactants since the substrates possess the same surface charge (both positively and negatively charged at pH value of 5 and 11, respectively).[26] Therefore, in acidic conditions, anionic AOT surfactant changes the surface charge of Cu_2O in order to self-assembly with positively charged TiO_2. An analogous procedure, with the use of cationic CTAB surfactant has been applied in basic conditions. The samples prepared in basic conditions show higher activity, and thus this manuscript presents these samples.

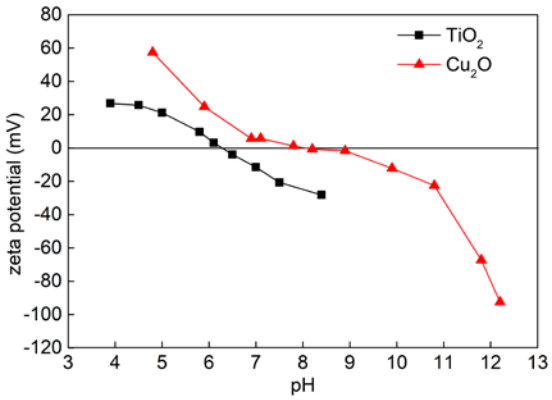

Fig. 1 Zeta potential as a function of pH value of Cu_2O and TiO_2 (ST01) suspensions.

Characterization of $Cu_2O@TiO_2$ samples

DRS spectra of all modified and bare samples are shown in Fig. 2 (a-b). The absorption at UV range is due to the intrinsic interband absorption of titania (ca. 3.2 eV), whereas absorption at vis range is caused by copper presence. All $Cu_xO@TiO_2$ samples are colored, and the color intensity (from light blue till dark blue-grey) increases with the content of Cu_2O (Fig. 2 (c)), as confirmed by absorption spectra (Fig. 2 (a-b)). However, the spectra at vis range do not resemble the shape of Cu_2O absorption (intensive absorption in the range of 400-650 nm), except for 50 wt% $Cu_xO@TiO_2$ sample (not enough content of TiO_2 to fully cover the Cu_2O core, as shown in Figs. 3a-c and S3). Interestingly, samples prepared by grinding (same Cu_2O and TiO_2; previous study[9]) have shown different color (pink) and DRS spectra resembling Cu_2O absorption at vis range (clear peak with maximum at ca. 550 nm). Similarly, other reports on Cu_2O-modified photocatalysts have shown photoabsorption spectra correlating with Cu_2O absorption at vis range, e.g., for Cu_2O/TiO_2 [16, 35-38] and Cu_2O/Si [39] samples. Therefore, it is expected that mainly different forms of copper are responsible for vis absorption, i.e., i) in the range of 400-500 nm: mixed oxides of copper, i.e., Cu^+/Cu [40] and Cu_xO/TiO_2 (x:1-2, due to interfacial charge transfer (IFCT) from the valence band of TiO_2 to the Cu_xO),[41] and (ii) at the wavelengths longer than 500 nm: CuO,[42, 43] $Cu(OH)_2$ (blue samples),[44] and d-d transitions of Cu^{2+} species.[45] The most similar spectra (to data shown in Fig. 2 (a)) have been obtained by Park et al. for Cu_xO/TiO_2, prepared by annealing of $Cu@Cu_2O$ nanocomposite mixed with titania precursor ($TiCl_4$).[46] It has been suggested that the formation of heterojunction between Cu_xO and TiO_2 is responsible for vis absorption in the range of 400-600 nm, whereas absorption at 600-1000 nm is caused by the $^2E_g \rightarrow {}^2T_{2g}$ interband transitions in the Cu^{2+} clusters. Accordingly, it is proposed that the conditions during microemulsion method might influence the properties of less stable oxides than titania, such as Cu_2O, changing their oxidation state, and thus resulting in the formation of mixed-oxidation-state materials (as confirmed also by XPS data discussed in the following part).

The XRD patterns for all photocatalysts are shown in Fig. 2 (d), whereas the crystalline composition and crystallite sizes are listed in Table 1. Titania (ST01) is composed of anatase, as proven by clear peaks at ca. 25º, 37-39º, 48º, 52-55º, 62-63º, 74-76º and 82-83º, with fine crystallites of ca. 8.6 nm. In the case of bare Cu_2O and 50wt% Cu_2O samples, clear peaks for cubic cuprous oxide could be detected at 29.63º, 36.37º, 42.45º, 61.64º and 73.75º. For 10 wt% Cu_2O sample, only main {111} peak of Cu_2O could be observed in XRD pattern. However, for the samples with lower than 10wt% content of Cu_2O only highly enlarged patterns and Rietveld analysis could confirm the presence of copper species. It should be pointed out that the formation of core/shell structures with Cu_2O by the microemulsion method does not influence the crystalline properties of titania, as expected since titania is well known for high chemical and thermal stability. However, a decrease in crystalline size of Cu_2O has been observed (from 88 nm till 54 nm), probable as a result of alkaline treatment (pH value change during microemulsion method). The crystalline content of titania in the coupled samples correlates well with that used for samples' preparation, i.e., reaching 99.1%, 98.8%, 95.5%, 88.8% and 57.9% of TiO_2 for 1%, 2%, 5%, 10% and 50%$Cu_xO@TiO_2$ samples, respectively.

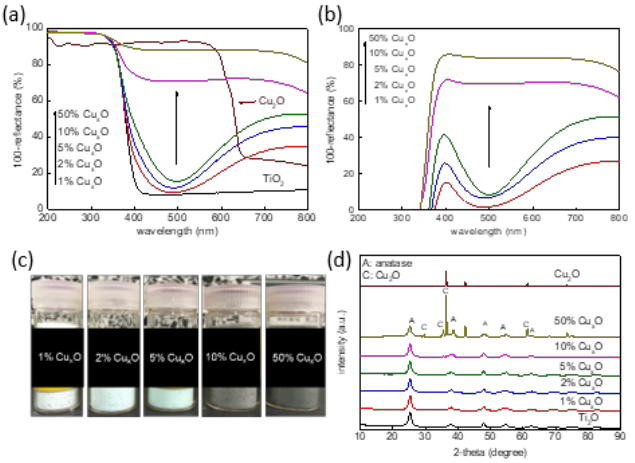

Fig. 2 Properties of samples: (a-b) DRS spectra taken with $BaSO_4$ (a) and bare TiO_2 (b) as reference; c) photograph of samples; d) XRD patterns.

Morphology of samples has been investigated by STEM microscopy with EDS mapping, and obtained results are shown in Figs. 3-4 and S1-3 (ESI). It should be reminded that commercial samples of TiO_2 and Cu_2O have been used for core/shell preparation, and thus without controlled morphology. Although, similar sizes of titania NPs could be clearly seen (9-20 nm, and aggregated NPs up to 60 nm (Fig. S4)), cuprous oxide is characterized by high polydispersity in the size (10 – 1000 nm (Fig. S4)) and the shape, including spherical and cubic particles, building-block structures and rods (Fig. S3)). One can distinguish two types of morphological configuration of analysed core/shell structures. The first one is composed of fine titania NPs localized on large Cu_xO particles (Figs. 3 (a and e-f) and S1-3), and the covering of Cu_2O depends on the content of titania, i.e., efficient coverage for 98 wt% (Figs. 3d-f and S1) and only partial for 50 wt% (Figs. 3a-c and S1). In the case of smaller Cu_xO particles of ca. 10 nm (possibly amorphous form undetected by XRD), they are also covered with fine titania, forming aggregated $Cu_xO@TiO_2$ particles (Fig. 3 (d)). Transmission electron (TE) image of 1wt% $Cu_xO@TiO_2$ sample has also confirmed the coverage of Cu_2O by a thick and porous shell of titania (in the form of aggregated core/shells), and with fine Cu_2O NPs in the range of 3-20 nm. On the other hand, 5 wt% Cu_2O sample has exhibited the thinner layer of titania (Fig. 4 and S2), which is reasonable considering the lower content of TiO_2, as clearly shown by distribution of shell thickness in Fig. S4.

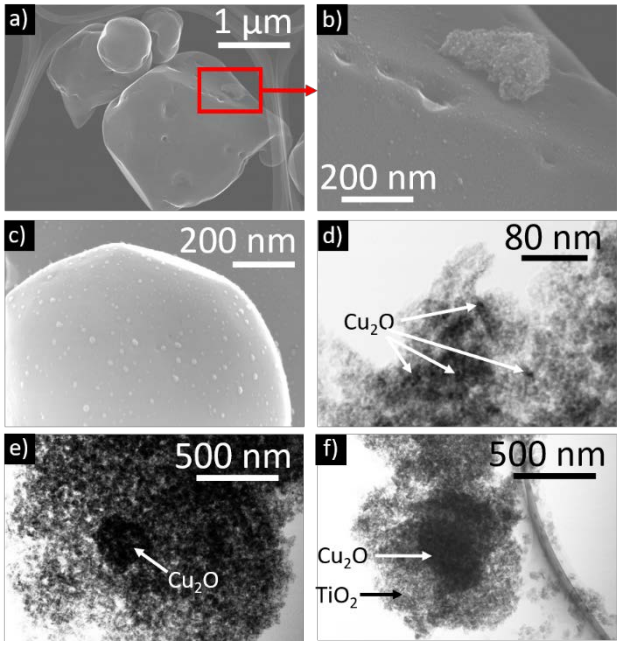

Fig. 3 STEM images of $Cu_xO@TiO_2$ samples with different Cu_2O content: 50 wt% (a-c), 2 wt% (d-f).

The oxidation states of elements and surface composition of samples have been investigated by XPS, and deconvoluted data are shown in Fig. 5 and Table 2 (summarized in the next section including results after photocatalytic tests). Titanium exists in

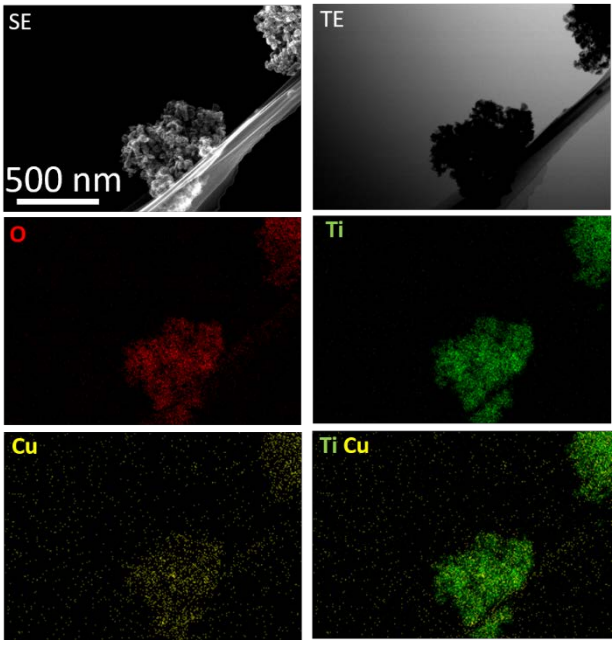

Fig. 4 STEM images with EDS mapping for 5 wt% Cu_xO sample: oxygen (red), titanium (green), copper (yellow).

Table 1 The properties of bare and composite samples

sample	color	TiO_2 (anatase)		Cu_2O		specific surface area
		(%)*	size (nm)	(%)*	size (nm)	$m^2\ g^{-1}$
TiO_2	white	100	8.6	-	-	310.8
Cu_2O	red	-	-	100	87.9	2.6
$1\%Cu_xO@TiO_2$	light blue	99.1	8.6	0.9	72.4	202.4
$2\%Cu_xO@TiO_2$	light blue	98.8	8.6	1.2	54.4	251.2
$5\%Cu_xO@TiO_2$	blue	95.5	8.6	4.7	68.0	238.3
$10\%Cu_xO@TiO_2$	blue/grey	88.8	8.3	11.2	60.4	231.3
$50\%Cu_xO@TiO_2$	dark blue/grey	57.9	8.2	42.1	63.6	170.4

(%)* - crystalline content in wt%; All crystallite sizes were analyzed from main peak in XRD patterns.

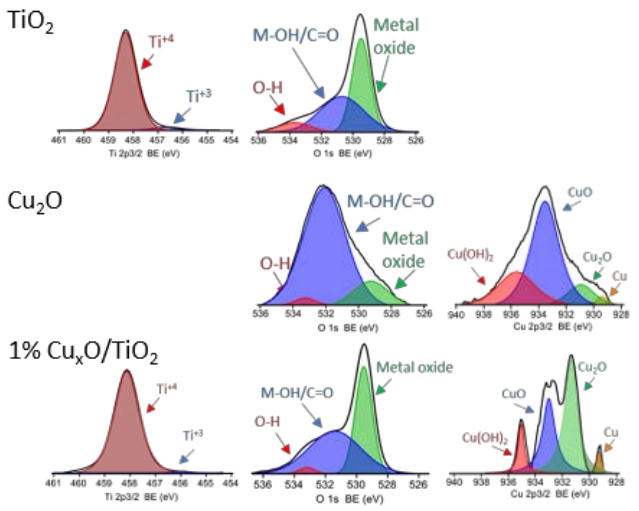

Fig. 5 XPS spectra for Ti $2p_{3/2}$, O 1s and Cu $2p_{3/2}$ of bare TiO_2 (1st line) Cu_2O (2nd line), and 1 wt%$Cu_xO@TiO_2$ (3rd line) samples.

mainly TiO_2 form (Ti^{4+}), but low content of reduced titanium (Ti^{3+}) has also been detected, reaching ca. 5%. The formation of core-shell structure results in a decrease in the content of Ti^{3+} till 0.8%. Accordingly, it is proposed that Ti^{3+} could be an active site for bonding with Cu_xO core, similar to surface titania modification with other elements/compounds, e.g., noble metals,[47] rare-earth elements[48] and ruthenium complexes.[49] Moreover, the content of hydroxyl groups on the titania surface (red part in oxygen spectrum) has decreased, which indicates that some hydroxyl groups participate in the core-shell formation. In the case of copper, the main peak at ca. 532 eV matches with Cu-OH, whereas Cu-O appears at lower energy of ca. 529 eV.[50] The oxygen peak for 1 wt%$Cu_xO@TiO_2$ sample could well resemble the respective counterparts, i.e., Cu_2O and TiO_2, considering the low content of Cu_2O. In the case of copper peak, four peaks might be estimated, i.e., CuO, $Cu(OH)_2$, Cu_2O and zero-valent Cu, reaching ca. 26.7%, 59.0%, 12.5% and 1.8%, respectively. The co-existence of various form of copper on the surface of commercial sample is not surprising since it is well known that Cu_2O is reactive and easily oxidized. Interestingly, in the core@shell particles, the content of Cu_2O has significantly increased, reaching ca. 45%. Accordingly, it is proposed that alkaline treatment during sample preparation has resulted in dissolution of surface layer (containing Cu^{2+}), leaving mainly Cu_2O as a core. Nevertheless, the mixed composition of copper forms has been confirmed (as suggested from DRS spectra), and thus the photocatalysts have been re-named as $Cu_xO@TiO_2$ (instead of $Cu_2O@TiO_2$).

For detailed characterization of photocatalysts, the reversed double-beam photo-acoustic spectroscopy (RDB-PAS) has been used. Bare and modified titania (ST01) samples, i.e., with 1wt% and 5wt% Cu_2O, prepared by two methods, i.e., microemulsion (this study: "@" samples) and physical mixing (grinding: "/" samples; previous study)[13] have been investigated, and obtained results are shown in Fig. 6. It has been proposed that conduction band bottom (CBB), energy-resolved distribution of electron traps (ERDT) patterns and total electron-trap (ET) density might reflect the bulk structure, surface structure and bulk/surface size, respectively.[51] Interestingly, only samples prepared as core@shells exhibit slight narrowing of bandgap (energy shift of conduction band bottom (CBB)), probably due to IFCT (as discussed earlier - DRS data). The ERDT patterns of bare TiO_2, 1% and 5% $Cu_xO@ST01$ clearly show that titania modification with Cu_2O has induced the shift of ETs (electron traps) inside conduction band in dependence of Cu_2O content (Fig. 6 (a)). On the basis of principle of RDB-PAS measurement, in which electrons in valence band of a sample is excited directly to ETs, and the density of electron-filled traps is measured, such high-energy shift of ERDT (energy-resolved distribution of electron traps) to higher energy side is quite unusual and might be attributable to, at least, two phenomena. (1) Some treatment of sample (during core/shell preparation) causes the change in the sample structure to induce a disappearance of lower energy traps and an appearance of higher energy traps. (2) The treatment causes coverage of sample surface to inhibit the contact with methanol, used as a hole-trapping agent in RDB-PAS measurement. Since, during RDB-PAS analysis, a light beam for excitation is scanned from higher energy side to lower energy side, when methanol supply is limited, the signal accumulation might be delayed, resulting in higher-energy shift of ERDT peak.

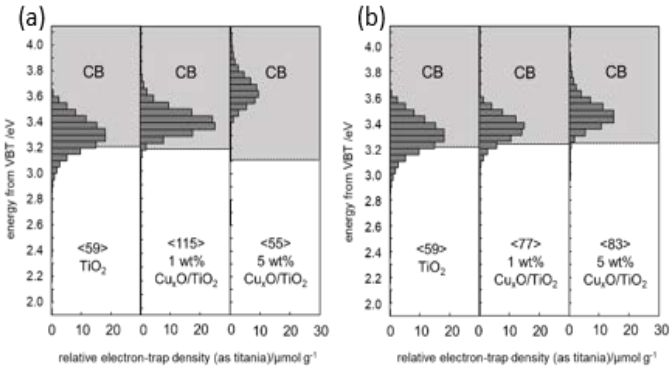

Fig. 6 ERDT patterns (bars) and CBB positions (bottom of grey box) for bare TiO_2, cores-shell (a) and physically mixed-ground (b) samples containing 1 wt% and 5 wt% of Cu_xO; values in < > denote the total density of ETs in the unit of μmol g^{-1}.

Nevertheless, the total ET density of 1%$Cu_xO@TiO_2$ sample is much higher (almost double) than that in other samples. It should be noted that it has been proposed that shallow ETs with high energy might be responsible for high photocatalytic activity.[52, 53] In addition, it must be reminded that the total ET density might reflect the specific surface area (SSA),[51] and thus an increase in specific surface area should result in enhanced photocatalytic activity.[30] Interestingly, the ground-mixed samples (1% and 5% Cu_2O/TiO_2) have shown similar tendency (Fig. 5 (b)), i.e., the higher the content of Cu_2O is, the deeper is ETs distribution inside CB. Moreover, the 5%Cu_2O/TiO_2 sample with the highest total ET density (83 μmol g^{-1}) and the deepest ETs distribution inside CB has shown the highest activity in both reaction systems under UV/vis irradiation, i.e., H_2 and CO_2 evolution.[13] In the present study, the most active samples for H_2

and CO_2 evolution (discussed in the next section) are 1%Cu_xO@TiO_2 and 5%Cu_xO@TiO_2 samples, respectively. Accordingly, it might be proposed that total ET density (in the case of high energy traps) and the shift of ERDT peak to higher energy might result in efficient reduction and oxidation reactions, respectively.

Activity of Cu_2O@TiO_2 samples

Photocatalytic activities of samples have been tested under UV/vis irradiation in two systems, i.e., oxidative decomposition of acetic acid with CO_2 evolution (CO_2 system) and dehydrogenation of methanol with H_2 evolution (H_2 system), and obtained data are shown in Fig. 7.

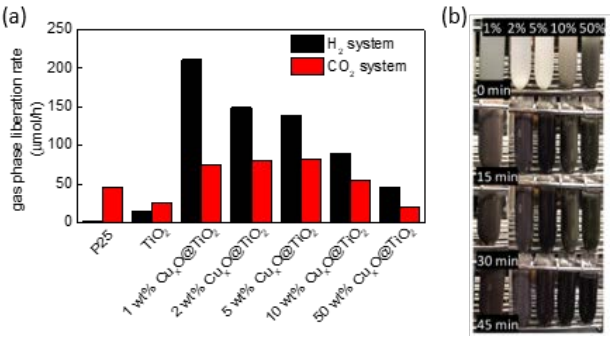

Fig. 7 Photocatalytic activity of samples under UV-vis irradiation in H_2 system and CO_2 system (a), the photographs of samples' color changes (b) during irradiation (from the top: 0, 15, 30 and 45 min of irradiation) in H_2 system.

The low activity of bare titania (ST01 and P25) in H_2 system (black bars) is not surprising since titania needs co-catalyst for efficient H_2 evolution. Although usually zero-valent noble metals (NPs or nanoclusters) have been used as co-catalysts,[47, 51, 54] other compounds have also been successfully applied, e.g., graphene,[53] Cu_2O [13] and Cu_xO.[14, 55] Similarly, Cu_xO@TiO_2 core/shell photocatalysts exhibit high photocatalytic activity for H_2 evolution, and the sample with the lowest content of Cu_xO has been the most active. Interestingly, the samples prepared by grinding (previous study)[13] have also shown high activity enhancement after Cu_2O addition, but the best performance has been obtained for larger content of Cu_2O, i.e., 5wt%. It should be pointed out that in ground samples, Cu_2O was the predominant form of copper (pink sample) and the irregular mixed-oxide structure has been formed. Here, the formation of core/shell structure with porous titania layer is highly beneficial for photocatalytic performance, reaching ca. 1.5 times higher activity that that by the most active ground sample.

Two possible mechanisms of enhanced activity by Cu_xO@TiO_2 photocatalysts have been proposed, i.e., electron transfer via type-II heterojunction and charges' separation in Z-scheme mechanism. In the case of heterojunction type II (Fig. 8 (a)), the electron transfer from CB of Cu_xO into CB of TiO_2, and reverse hole transfer (i.e., from VB of TiO_2 into VB of Cu_2O) might result in efficient charge carriers' separation, but also in lower redox ability (electrons in less negative CB and holes in less positive VB). Therefore, Z-scheme mechanism with recombination of electrons from TiO_2 and holes from Cu_2O (Fig. 8 (b)) is preferable for efficient redox reactions. It should be

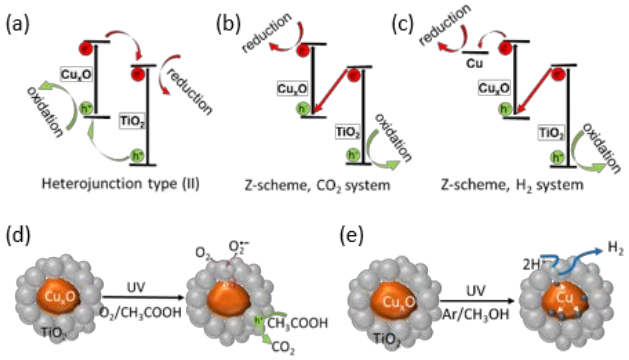

Fig. 8 The schematic drawings of: a) heterojunction type II between Cu_xO and TiO_2, b) basic Z-scheme mechanism of charge transfer between Cu_xO and TiO_2, c) modified Z-scheme mechanism of charge transfer between Cu_xO and TiO_2 with participation of zero-va valent Cu, d) oxidative decomposition of acetic acid on porous Cu_xO@TiO_2 photocatalyst, and e) methanol dehydrogenation on porous Cu_xO@TiO_2 photocatalyst with simultaneous formation of zero-valent Cu.

reminded that Cu_xO has been used as a core, and thus the change of oxidation state of copper might confirm the mechanism of action, i.e., oxidation and reduction of copper should indicate heterojunction type II and Z-scheme, respectively. Indeed, XPS analysis (Fig. 9 and Table 2) performed after prolonged irradiation (8-h; stability study discussed in the following part; Fig. 11) suggests that copper has been reduced, resulting in the formation of the sample with the high content of zero-valent copper (an increase from ca. 4 to 28%), as shown by color change of samples (Fig. 7 (b)) and schematic drawings in Fig. 8 (c-d). Wang et al. have found similar reduction of copper (XAFS analysis) even for copper NPs deposited on the titania surface during H_2 generation under UV irradiation, i.e., from Cu^{2+} via Cu^+ to Cu^0.[56] Additionally, it should be pointed out that zero-valent copper is not stable (due to fast oxidation), and thus obtained XPS data have confirmed that the core@shell structure has been formed, keeping metallic copper safely inside titania porous layer. However, it is also expected that proton reduction might be impossible on the surface of copper when it is inside the titania shell. Therefore, it has been proposed that the titania layer is not compact, but rather composed of fine NPs, resulting in the formation of highly porous layer, permittable for small atoms/molecules (e.g., H^+/H_2), as shown in Fig. 8e. Additionally, considering the dark colorations of samples during irradiation (the formation of zero-valent copper), the highest activity of the sample with the lowest content of copper should be caused by the less dark color. It is clear that light transmittance through such dark suspensions is hindered (the shielding effect; similar for Pt/TiO_2),[51] and thus only part of sample is photo-activated by incident light.

In the case of CO_2 system, the photocatalytic activity of almost all coupled samples (except 50 wt%) has been significantly increased after titania modification with Cu_2O, reaching almost three times higher activity (for 1-5 wt% Cu_xO samples) than that by bare titania. It should be pointed out that the color of samples has not changed significantly during short

(60 min) irradiation in the case of aerobic conditions, and thus the photocatalytic activity might mainly correlate with specific surface area (SSA). It is well-known that larger SSA results in more efficient adsorption of reagents, and thus faster reactions, especially in CO_2 system, which has already been confirmed by systematic studies performed on more than 40 titania samples in different reaction systems.[30] Indeed, significant activity drop has been obtained for the sample with reduced SSA, i.e., containing of 50 wt% of Cu_xO. Like H_2 system, both mechanisms (Z-scheme and II-type heterojunction; Fig. 8 a-b) should be considered in CO_2 system. XPS data (Fig. 9) have confirm that also in the case of oxidation reaction, copper has been reduced. Accordingly, Z-scheme has been proven in both reaction systems under UV irradiation, confirming efficient formation of core@shell structure, which prevents the photo-corrosion of Cu_xO and its leakage.

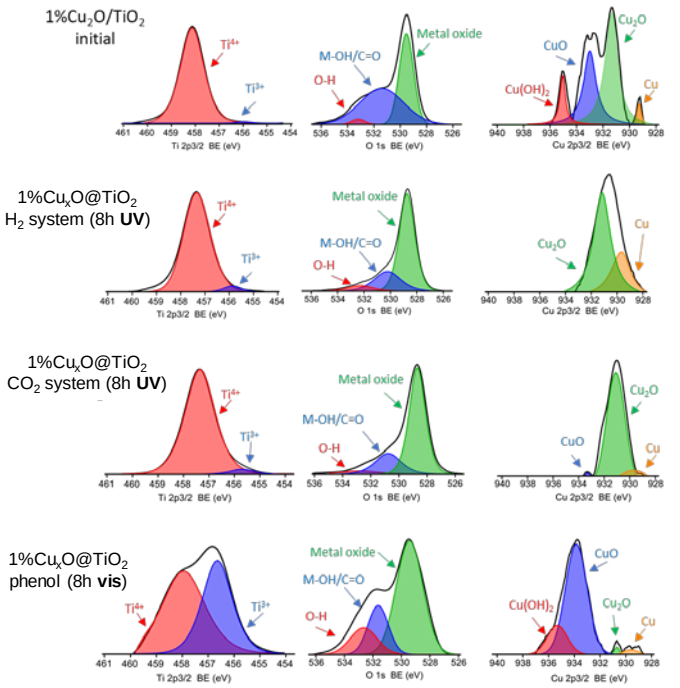

Fig. 9 XPS spectra for Ti $2p_{3/2}$, O 1s and Cu $2p_{3/2}$ of 1%$Cu_xO@TiO_2$ sample before (1st line; same data as that in Fig. 3) and after 8-h irradiation during: methanol dehydrogenation under UV (2nd line), acetic acid oxidation under UV (3rd line) and phenol oxidation under vis (4th line).

For CO_2 system, oxidation of acetic acid might proceed by two pathways, i.e., via i) photo-generated holes in TiO_2 and/or ii) superoxide ion ($O_2^{\bullet-}$) formed from O_2 reduction by electrons from Cu_xO. Since the photocatalysts show high stability (Figs. 11b and 12b; discussed farther), it is expected that oxidation should also proceed by $O_2^{\bullet-}$ (If not the activity should be stopped since for efficient Z-scheme both an electron acceptor on Cu_xO core and an electron donor on TiO_2 shell is necessary.). In the case of $O_2^{\bullet-}$, two possibilities should be considered, i.e., i) the penetration of O_2 inside TiO_2 shell or ii) an electron transfer via TiO_2 network to adsorbed oxygen on the shell surface. It is proposed that the latter is more possible since oxygen is probably too large to penetrate via titania shell and due to negligible activity of samples under vis irradiation (lack of electron donor inside titania shell, as discussed in the next section). Accordingly, the electron transfer via titania shell has been proposed for efficient activity of core@shell photocatalysts in CO_2 system, as shown in Fig. 8e. This mechanism might also explain an increase in activity with an increase in Cu_xO content from 1 wt% to 5 wt% (99 wt% and 95 wt% of titania, respectively), resulting from the formation of core@shell particles with thinner titania shell, and thus allowing fast electron transfer via TiO_2 network. Moreover, the experiments in the presence of different scavengers (Fig. S5 in ESI) have confirmed that $O_2^{\bullet-}$ radicals are mainly responsible for oxidative decomposition of acetic acid, i.e., activity has dropped by ca. 50% in the presence of 4-hydroxy-2,2,6,6-tetramethylpiperidin-1-oxyl (TEMPOL). It should be mentioned that isopropanol as $HO^{\bullet}$ scavenger has also decreased activity significantly (by ca. 30%), which might also indirectly confirm Z-scheme mechanism.

Since all coupled samples have been coloured, the photocatalytic activity under vis irradiation has also been tested for oxidative decomposition of phenol as a model compound. It must be pointed out that a disappearance of phenol (concentration decrease in an aqueous phase) is not equal with its degradation, but also could be caused by its adsorption on the photocatalyst surface (as confirmed by 30-min pre-stirring in the dark), and thus the determination of oxidation products is highly recommended. Consequently, activity data are presented for both: (i) a decrease in the phenol concentration (Fig. 10 (a)) and (ii) formation of main intermediate, i.e., benzoquinone (Fig. 10 (b)). In the case of vis activity, only Cu_xO could be excited, and thus the mechanism of type-II heterojunction with only Cu_xO excitation should be considered, i.e., an electron transfer from CB of Cu_xO into CB of TiO_2. Accordingly, oxidation of organic compounds (here phenol) could proceed on the titania surface. However, for efficient and stable photocatalytic performance of Cu_xO, both redox reactions should take place, i.e., reduction and oxidation. In the case of Cu_xO core, there is no any hole acceptor inside titania shell, and thus the photogenerated holes first are self-oxidizing Cu_xO core, as confirmed by change of oxidation state of copper ($Cu^+ \rightarrow Cu^{2+}$; Fig. 9 and Table 2), and then no further reaction might occur. Interestingly, an electron transfer from Cu_xO into TiO_2 has also been confirmed by XPS data for titanium since significant reduction of Ti^{4+} has been noticed (Ti^{3+} content increase from ca. 1 to 50%). Indeed, the obtained data has confirmed negligible vis-response of $Cu_xO@TiO_2$ core/shell photocatalysts. Interestingly, bare commercial TiO_2 (P25) exhibits even higher vis response than core@shell photocatalysts, which might be cause by ETs presence inside bandgap. The slight vis-response for commercial and faceted

Table 2 Surface composition of samples after deconvolution of XPS peaks

samples	Ti		O			Cu			
	Ti^{3+}	Ti^{4+}	O-H	M-OH/C=O	metal oxide	$Cu(OH)_2$	CuO	Cu_2O	Cu
TiO_2	5.1	94.9	5.3	34.2	60.5	-	-	-	-
Cu_2O	-	-	7.5	61.9	30.6	26.7	59.0	12.5	1.8
1%Cu_xO@TiO_2 initial	0.8	99.2	1.7	54.1	44.2	10.2	40.5	45.4	3.9
1%Cu_xO@TiO_2 8h H_2 (UV)	3.3	96.7	4.4	25.1	70.5	-	-	71.2	28.8
1%Cu_2O@TiO_2 8h CO_2 (UV)	3.4	96.6	4.5	21.5	74.0	-	2.9	89.7	7.4
1%Cu_xO@TiO_2 8h (vis)	49.7	50.3	15.2	23.4	61.4	16.4	68.3	1.5	13.8

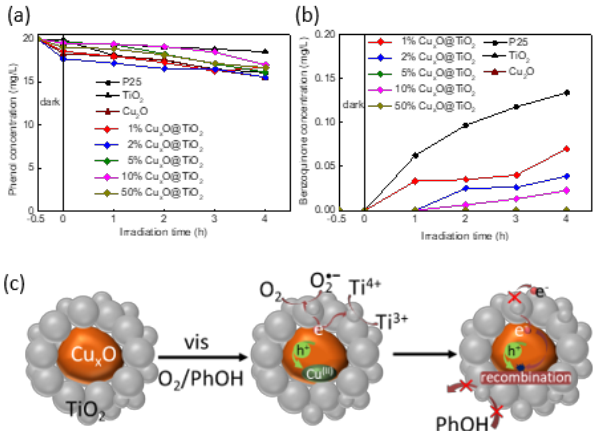

Fig. 10 Vis-activity of bare samples and coupled photocatalysts as the rate of phenol disappearance (a), and the rate of benzoquinone generation (b), and the possible mechanism under vis irradiation (c).

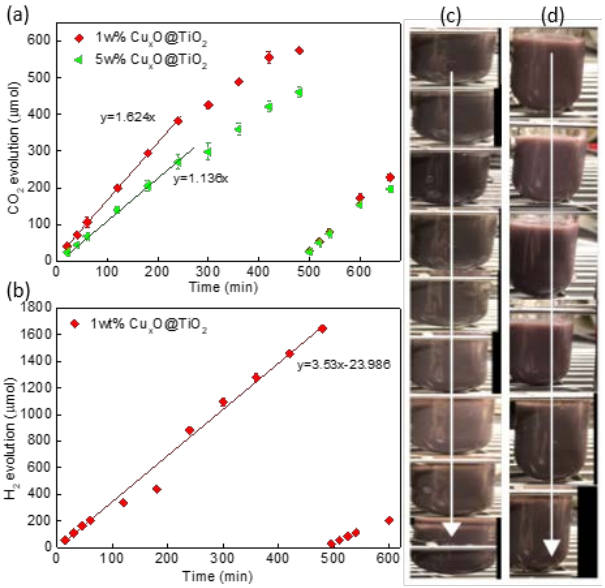

Fig. 11 Long-term photocatalytic activity of samples in: a) CO_2 system for 1 wt% and 5 wt% Cu_xO@TiO_2 samples, and b) H_2 system for 1 wt%Cu_xO@TiO_2, and c-d) photographs of samples during irradiation in H_2 system: c) first irradiation (after: 0, 1, 2, 3, 4, 5, 6, 7 and 8-h irradiation (from the top)), d) second irradiation (after: 0, 15 min, 30 min, 45 min, 1 h and 2 h of irradiation (from the top)).

titania samples with shallow ETs has already been reported,[57] and the defect-rich titania ("self-doped") has been proposed as efficient vis-responsive materials.[58]

In order to check the stability of samples, long-term photocatalytic activity has been investigated, and the results are shown in Fig 11. Since high accumulation of gas products (H_2 and CO_2) inside the testing tubes during 8-h irradiation and insufficiency of dissolved oxygen in CO_2 system have been observed, the testing tubes have been re-opened, purged with Ar or air (in the case of H_2 and CO_2 system, respectively) and once more irradiated for next 120 min and 180 min, respectively.

The stable activity has been observed in CO_2 system during 4 h of irradiation for fresh and pre-irradiated samples (Fig. 11 (a)). The extended irradiation (> 4h) has caused a slight decrease in reaction rate, because of insufficient content of dissolved oxygen, which has been confirmed by re-increase in reaction rate during the subsequent irradiation of air-bubbled samples. Accordingly, it is proposed that even when surface state of copper has changed during irradiation from Cu^{2+} into mainly Cu^{+}, the stable activity without sample discoloration has been achieved. In the case of H_2 system, although stable activity has been observed during 8-h irradiation (Fig. 11 (b)), opening of the testing tube and Ar-bubbling has caused a decrease in reaction rate by about a half. Therefore, it is proposed that small content of copper (e.g., as Cu^{+} or Cu^{0} clusters) could also penetrate through the titania layer, acting as a co-catalyst on its surface for H_2 evolution. However, post-bubbling could cause their detachment from the photocatalyst surface, and thus re-irradiated sample has shown lower activity, resulting from less content of active sites for H_2 evolution. This hypothesis could be confirmed by slight colour change of samples during irradiation, i.e., i) slight discoloration during first irradiation (loss of copper species; Fig 11 (c)), and ii) stable colour during re-irradiation (no more copper leakage from the photocatalyst surface; Fig 11 (d)). Accordingly, it is proposed that even if little loss of activity in the initial stage of photocatalytic process could be observed (by imperfect Cu_xO coverage with TiO_2 layer), the coupled photocatalysts are quite stable, and could be successfully applied for photocatalytic reactions under UV irradiation. It should be pointed out that samples prepared by grinding has

not been stable at all with complete discoloration during longer irradiation.[13]

To further improve the stability of core@shell particles and to avoid any possibilities of copper leakage, thermal treatment was applied. At first, the condition of annealing was optimized, i.e., 2 h at 180 °C, for bare Cu_2O sample to avoid oxidation of cuprous to cupric oxide. Accordingly, 1 wt% $Cu_xO@TiO_2$ core@shell sample was heated, and then tested during three photocatalytic cycles in both reaction systems, and obtained data are shown in Fig. 12. It might be concluded that post-treatment by annealing results in successful preparation of stable photocatalysts during long-term irradiation and recycling.

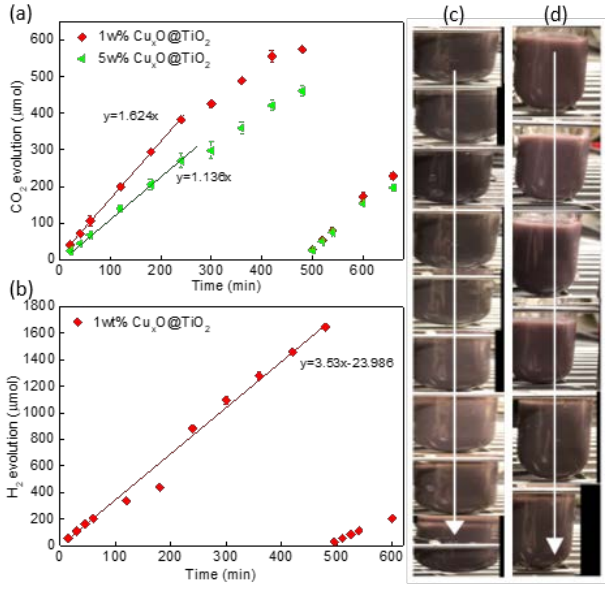

Fig. 12 Long-term photocatalytic activity of thermally treated (2 h, 180 °C) 1 wt% $Cu_xO@TiO_2$ sample in: a) CO_2 system, and b) H_2 system.

4. Conclusions

Microemulsion method has proven to be an efficient way for the preparation of $Cu_xO@TiO_2$ core/shell photocatalysts. However, the alkaline conditions during samples' preparation result in the change of oxidation state of copper (mixed-oxidation states) and in a decrease in Cu_xO size. Nevertheless, the core@shell structure guarantees the high stability under UV irradiation (especially after annealing), in contrast to simply mixed oxides (Cu_2O/TiO_2), independently on the kind of redox reaction (both for oxidation and reduction). Moreover, the change of surface charges of copper core indicates the Z-scheme mechanism, which is the main reason of high efficiency of $Cu_xO@TiO_2$ photocatalyst. The core@shell particles have only one, but quite serious shortcoming, i.e., negligible activity under vis irradiation. However, efficient reduction of copper oxides inside titania layer under UV irradiation, gives opportunity with the formation of stable and efficient vis-responsive material, i.e., plasmonic photocatalyst ($Cu^0@TiO_2$).

The above results unequivocally show that coupled $Cu_xO@TiO_2$ with core@shell nanostructure has a significant potential to be an efficient and stable photocatalyst dedicated to various reaction systems.

Conflicts of interest

There are no conflicts to declare.

Acknowledgements

Authors thank Professor Zhishun Wei (Hubei University of Technology, China) for fruitful discussion on samples' characterization. This research has been financially supported by Polish National Science Centre (2016/21/B/ST5/03387) and "Yugo-Sohatsu Kenkyu" for an Integrated Research Consortium on Chemical Sciences (IRCCS) project from the Ministry of Education and Culture, Sport, Science and Technology-Japan (MEXT).

References

1. J. Schneider, M. Matsuoka, M. Takeuchi, J. Zhang, Y. Horiuchi, M. Anpo and D. W. Bahnemann, *Chem. Rev.*, 2014, **114**, 9919-9986.
2. M. Pelaez, N. T. Nolan, S. C. Pillai, M. K. Seery, P. Falaras, A. G. Kontos, P. S. M. Dunlop, J. W. J. Hamilton, J. A. Byrne, K. O'Shea, M. H. Entezari and D. D. Dionysiou, *Appl. Catal. B-Environ.*, 2012, **125**, 331-349.
3. X. Chen, S. Shen, L. Guo and S. S. Mao, *Chem. Rev.*, 2010, **110**, 6503-6570.
4. X. Li, J. Yu, M. Jaroniec and X. Chen, *Chem. Rev.*, 2019, **119**, 3962-4179.
5. M. Kobielusz, P. Mikrut and W. Macyk, in *Materials for Sustainable Energy*, eds. R. van Eldik and W. Macyk, Academic Press, 2018, vol. 72, pp. 93-144.
6. N.B. McGuinness, H. John, M.K. Kavitha, S. Banerjee, D.D. Dionysiou, S.C. Pillai, *Photocatalysis: Applications*, Royal Society of Chemistrym 2016, chapter 8, 204-231.
7. K. Wang, M. Janczarek, Z. Wei, T. Raja-Mogan, M. Endo-Kimura, T. M. Khedr, B. Ohtani and E. Kowalska, *Catalysts*, 2019, **9**, 30.
8. Y. Bessekhouad, D. Robert and J. V. Weber, *J. Photoch. Photobio. A*, 2004, **163**, 569-580.
9. M. Janczarek and E. Kowalska, *Catalysts*, 2017, **7**.
10. M. Muscetta, R. Andreozzi, L. Clarizia, I. Di Somma and R. Marotta, *Int. J. Hydrogen Energ.*, 2020, **45**, 28531-28552.
11. L. Huang, F. Peng, H. Wang, H. Yu and Z. Li, *Catal. Commun.*, 2009, **10**, 1839-1843.
12. S. S. Zhang, B. Y. Peng, S. Y. Yang, Y. P. Fang and F. Peng, *Int. J. Hydrogen Energ.*, 2013, **38**, 13866-13871.
13. M. Janczarek, M. Endo, D. Zhang, K. Wang and E. Kowalska, *Materials (Basel)*, 2018, **11**.
14. G. Vitiello, L. Clarizia, W. Abdelraheem, S. Esposito, B. Bonelli, N. Ditaranto, A. Vergara, M. Nadagouda, D. D. Dionysiou, R. Andreozzi, G. Luciani and R. Marotta, *ChemCatChem*, 2019, **11**, 4314-4326.
15. Z. Zheng, B. Huang, Z. Wang, M. Guo, X. Qin, X. Zhang, P. Wang and Y. Dai, *J. Phys. Chem. C*, 2009, **113**, 14448-14453.

16. C. Y. Toe, Z. Zheng, H. Wu, J. Scott, R. Amal and Y. H. Ng, *Angew. Chem. Int. Ed.*, 2018, **57**, 13613-13617.
17. P. Wang, X. Wen, R. Amal and Y. H. Ng, *RSC Adv.*, 2015, **5**, 5231-5236.
18. W. Li, A. Elzatahry, D. Aldhayan and D. Zhao, *Chem. Soc. Rev.*, 2018, **47**, 8203-8237.
19. R. Ghosh Chaudhuri and S. Paria, *Chem. Rev.*, 2012, **112**, 2373-2433.
20. Z. Bielan, E. Kowalska, S. Dudziak, K. Wang, B. Ohtani and A. Zielinska-Jurek, *Catal. Today*, 2020, DOI: 10.1016/j.cattod.2020.05.034, in press.
21. A. Zielinska-Jurek, Z. Bielan, I. Wysocka, J. Strychalska, M. Janczarek and T. Klimczuk, *J. Environ. Manage.*, 2017, **195**, 157-165.
22. X. D. Su, J. Z. Zhao, Y. L. Li, Y. C. Zhu, X. K. Ma, F. Sun and Z. C. Wang, *Colloid. Surface A*, 2009, **349**, 151-155.
23. W. Siripala, A. Ivanovskaya, T. F. Jaramillo, S.-H. Baeck and E. W. McFarland, *Sol. Energ. Mat. Sol. C*, 2003, **77**, 229-237.
24. A. Paracchino, V. Laporte, K. Sivula, M. Gratzel and E. Thimsen, *Nat. Mater.*, 2011, **10**, 456-461.
25. M. Schreier, P. Gao, M. T. Mayer, J. S. Luo, T. Moehl, M. K. Nazeeruddin, S. D. Tilley and M. Gratzel, *Energ. Environ. Sci.*, 2015, **8**, 855-861.
26. A. Zielińska-Jurek, Z. Bielan, S. Dudziak, I. Wolak, Z. Sobczak, T. Klimczuk, G. Nowaczyk and J. Hupka, *Catalysts*, 2017, **7**.
27. T. Luttrell, S. Halpegamage, J. Tao, A. Kramer, E. Sutter and M. Batzill, *Sci. Rep.*, 2014, **4**, 4043.
28. M. P. Pileni, *J. Phys. Chem.*, 1993, **97**, 6961-6973.
29. N. R. Zia Ul Haq, Farman Ali, Nasir Mehmood Khan, Hidayat Ullah, *J. Mat. Environ. Sci.* 2017, **8**, 1029-1038.
30. O.-O. Prieto-Mahaney, N. Murakami, R. Abe and B. Ohtani, *Chem. Lett.*, 2009, **38**, 238-239.
31. M. Buchalska, M. Kobielusz, A. Matuszek, M. Pacia, S. Wojtyla and W. Macyk, *ACS Catal.*, 2015, **5**, 7424-7431.
32. M. A. Ferguson and J. G. Hering, *Environ. Sci. Technol.*, 2006, **40**, 4261-4267.
33. B. Neppolian, H. C. Choi, S. Sakthivel, B. Arabindoo and V. Murugesan, *J. Hazard. Mater.*, 2002, **89**, 303-317.
34. H. Sakai, Y. Kubota, K. Yamaguchi, H. Fukuoka and K. Inumaru, *J. Porous Mater.*, 2012, **20**, 693-699.
35. M. Janczarek, K. Wang and E. Kowalska, *Catalysts*, 2018, **8**.
36. Y. Liu, Q. Huang, G. Jiang, D. Liu and W. Yu, *J. Mater. Res.*, 2017, **32**, 3605-3615.
37. Y. Bessekhouad, D. Robert and J. V. Weber, *Catal. Today*, 2005, **101**, 315-321.
38. J. Zhang, W. Liu, X. Wang, X. Wang, B. Hu and H. Liu, *Appl. Surf. Sci.*, 2013, **282**, 84-91.
39. C. H. Tang, P. H. Hsiao and C. Y. Chen, *Nanoscale Res. Lett.*, 2018, **13**, 312.
40. A. T. Montoya and E. G. Gillan, *ACS Omega*, 2018, **3**, 2947-2955.
41. X. Qiu, M. Miyauchi, K. Sunada, M. Minoshima, M. Liu, Y. Lu, D. Li, Y. Shimodaira, Y. Hosogi, Y. Kuroda and K. Hashimoto, *ACS Nano*, 2012, **6**, 1609-1618.
42. M. G. Méndez-Medrano, E. Kowalska, A. Lehoux, A. Herissan, B. Ohtani, D. Bahena, V. Briois, C. Colbeau-Justin, J. L. Rodríguez-López and H. Remita, *J. Phys. Chem. C*, 2016, **120**, 5143-5154.
43. M. G. Méndez-Medrano, E. Kowalska, M. Endo-Kimura, K. Wang, B. Ohtani, D. Bahena Uribe, J. L. Rodríguez-López and H. Remita, *ACS Appl. Bio Mater.*, 2019, **2**, 5626-5633.
44. J. Yu and J. Ran, *Energ. Environ. Sci.*, 2011, **4**, 1364-1371.
45. N. L. Dias Filho, *Mikrochim. Acta*, 1999, **130**, 233-240.
46. S. M. Park, A. Razzaq, Y. H. Park, S. Sorcar, Y. Park, C. A. Grimes and S. I. In, *ACS Omega*, 2016, **1**, 868-875.
47. Z. Wei, M. Endo, K. Wang, E. Charbit, A. Markowska-Szczupak, B. Ohtani and E. Kowalska, *Chem. Eng. J.*, 2017, **318**, 121-134.
48. P. Mazierski, P. N. A. Caicedo, T. Grzyb, A. Mikolajczyk, J. K. Roy, E. Wyrzykowska, Z. S. Wei, E. Kowalska, T. Puzyn, A. Zaleska-Medynska and J. Nadolna, *Appl. Catal. B-Environ.*, 2019, **252**, 138-151.
49. S. Zheng, Z. Wei, K. Yoshiiri, M. Braumuller, B. Ohtani, S. Rau and E. Kowalska, *Photochem. Photobiol. Sci.*, 2016, **15**, 69-79.
50. Z. Dan, Y. Yang, F. Qin, H. Wang and H. Chang, *Materials (Basel)*, 2018, **11**.
51. K. Wang, Z. Wei, B. Ohtani and E. Kowalska, *Catal. Today*, 2018, **303**, 327-333.
52. B. Ohtani, O. O. Prieto-Mahaney, D. Li and R. Abe, *J. Photochem. Photobio. A: Chem.*, 2010, **216**, 179-182.
53. K. Wang, M. Endo-Kimura, R. Belchi, D. Zhang, A. Habert, J. Boucle, B. Ohtani, E. Kowalska and N. Herlin-Boime, *Materials (Basel)*, 2019, **12**.
54. M. Janczarek, Z. Wei, M. Endo, B. Ohtani and E. Kowalska, *J. Photon. Energy*, 2016, **7**, 16.
55. M. Jung, J. Scott, Y. H. Ng, Y. Jiang and R. Amal, *Int. J. Hydrogen Energ.*, 2014, **39**, 12499-12506.
56. Z. Wang, K. Teramura, T. Shishido and T. Tanaka, *Top. Catal.*, 2014, **57**, 975-983.
57. Z. Wei, M. Janczarek, M. Endo, K. L. Wang, A. Balcytis, A. Nitta, M. G. Mendez-Medrano, C. Colbeau-Justin, S. Juodkazis, B. Ohtani and E. Kowalska, *Appl. Catal. B-Environ.*, 2018, **237**, 574-587.
58. Q. P. Wu, F. Huang, M. S. Zhao, J. Xu, J. C. Zhou and Y. S. Wang, *Nano Energy*, 2016, **24**, 63-71.